Heme Photolysis Occurs by Ultrafast Excited State Metal-to-Ring Charge Transfer

Stefan Franzen,* Laurent Kiger,‡ Claude Poyart,‡ and Jean-Louis Martin†
*Department of Chemistry, North Carolina State University, Raleigh, North Carolina 27695, USA, †Laboratoire d'Optique Appliquée Institut Nationale de la Sante et de la Recherche Medicale, U275 Ecole Polytechnique-, 91120 Palaiseau, France, and
‡U299 Le Kremlin-Bicetre, France

ABSTRACT Ultrafast time-resolved resonance Raman spectra of carbonmonoxy hemoglobin (Hb), nitroxy Hb, and deoxy Hb are compared to determine excited state decay mechanisms for both ligated and unligated hemes. Transient absorption and Raman data provide evidence for a sequential photophysical relaxation pathway common to both ligated and unligated forms of Hb* (photolyzed heme), in which the excited state ^1Q decays sequentially: $^1Q \rightarrow Hb^*_I \rightarrow Hb^*_{II} \rightarrow Hb$ ground state. Consistent with the observed kinetics, the lifetimes of these states are <50 fs, ≈ 300 fs, and ≈ 3 ps for ^1Q, Hb^*_I, and Hb^*_{II}, respectively. The transient absorption data support the hypothesis that the Hb^*_I state results from an ultrafast iron-to-porphyrin ring charge transfer process. The Hb^*_{II} state arises from porphyrin ring-to-iron back charge transfer to produce a porphyrin ground state configuration a nonequilibrium iron d-orbital population. Equatorial d–π^* back-bonding of the heme iron to the porphyrin during the lifetime of the Hb^*_{II} state accounts for the time-resolved resonance Raman shifts on the ≈ 3 ps time scale. The proposed photophysical pathway suggests that iron-to-ring charge transfer is the key event in the mechanism of photolysis of diatomic ligands following a porphyrin ring $\pi - \pi^*$ transition.

INTRODUCTION

The photolysis of diatomic ligands from heme iron has been used to study ligand rebinding kinetics and protein relaxation processes in a number of heme proteins. Extensive comparisons of the rebinding kinetics of CO and NO have been made in mutant myoglobin leading to insight into the steric constraints to the ligand rebinding process (Carlson et al., 1994; Petrich et al., 1994). Evidence for rapid protein relaxation at ambient temperature has been presented (Jackson et al., 1994). Time-dependent x-ray structural studies and low-temperature photoproduct structures of carbonmonoxy myoglobin provide a structural picture that correlates with these spectroscopic observations (Hartmann et al., 1996; Schlichting et al., 1994; Srajer et al., 1996; Teng et al., 1994). Studies of heme photophysics provide important insight into the nature of photolysis as distinct from the physiological process of thermal ligand dissociation. It is desirable to understand whether local heating may affect ligand trajectories and protein dynamics on the picosecond time scale. Absorption band shifts in the heme that are important for interpretation of protein relaxation processes may have contributions from intramolecular vibrational relaxation and cooling (Gottfried and Kaiser, 1983; Kruglik et al., 1997; Lian et al., 1994; Lim et al., 1996; Mizutani and Kitagawa, 1997; Schneebeck et al., 1993; Sension et al., 1993). These aspects are important for all diatomic ligand recombination processes (CO, NO, and O_2 recombination) because protein relaxation is rapid compared to ligand recombination. However, there are important differences among these ligands. NO geminate recombination is nearly as rapid as heme photophysical relaxation and occurs essentially on the time scale of protein relaxation in buffered solutions at room temperature (Ahmed et al., 1991; Chance et al., 1990; Petrich et al., 1988). Diatomic oxygen has an extremely rapid recombination process for a minority population (25%). The origin of the differences in barriers to recombination for the diatomic ligands is still not understood. However, it is widely recognized that the CO and NO serve as excellent probes of protein dynamics on time scales from picoseconds to seconds. Studies of heme photophysics (Cornelius et al.; 1983, Martin et al., 1983b; Petrich et al., 1987) are key to understanding the nature of the barrier to ligand rebinding (Franzen et al., 1995b; Walda et al., 1994) and the mechanism of photolysis of diatomic π-acid ligands (Hoffman and Gibson, 1978).

Previous studies have demonstrated that heme photophysics is similar in hemoglobin (Hb), heme proteins, and heme model systems. All of these hemes exhibit two excited states designated Hb^*_I and Hb^*_{II} (Baldwin and Chothia, 1979; Franzen et al., 1995a,b; Martin et al., 1983a; Perutz, 1979; Petrich et al., 1988). The data show that Hb^*_I is formed in less than 50 fs and then decays to form Hb^*_{II} in 300 fs. The lifetime of the Hb^*_{II} electronic state is roughly 3 ps followed by recovery of the ground state. This electronic relaxation is sufficiently rapid that intramolecular vibrational redistribution (IVR) and vibrational cooling occur on a similar (or even slightly longer) time scale. Estimates for cooling and IVR range from 3 ps to tens of ps (Gottfried and Kaiser, 1983; Kruglik et al., 1997; Lian et al., 1994; Lim et al., 1996; Mizutani and Kitagawa, 1997; Schneebeck et al., 1993; Sension et al., 1993). In photolyzed Hb*CO or Hb*NO, any spectral differences observed on a time scale

Received for publication 22 May 2000 and in final form 30 January 2001.
Address reprint requests to Stefan Franzen, Department of Chemistry, North Carolina State University, P.O. Box 8204, Raleigh, NC 27695. Tel.: 919-515-8915; Fax: 919-515-8909; E-mail: stefan_franzen@ncsu.edu.

0006-3495/01/05/2372/14 $2.00

of longer than 10 ps can be attributed to conformational effects of protein relaxation. However, the interpretation of spectroscopic signals during the first 10 ps depends on the ability to separate photophysical processes of the heme from conformational effects. The first step in distinguishing photophysical processes from conformational contributions is to compare spectra of ligated species to deoxy species. However, differences in the photophysics of these species may exist due to the larger excess energy in deoxy Hb as compared with ligated hemoglobins. In photolyzed Hb*CO, at least 20 kcal/mol ($>$6400 cm^{-1}) is needed to break the Fe–CO bond (Keyes et al., 1971; Mills et al., 1979). Thus, a significant fraction of the energy of a photon required for excitation at 570 nm (17,500 cm^{-1}) is lost during the photolysis event. In spite of this energy difference, the electronic relaxation pathways of heme-CO and deoxy heme are thought to be similar (Petrich et al., 1988). Both the photodissociation of CO and the heme-iron movement out of plane occur very rapidly ($<$50 fs) to create a species that resembles deoxy Hb. Also, Hb_I^* transient spectra appear on the same time scale as photolysis in both Hb*CO and Hb*NO and the intensity and frequency of Hb_I^* in deoxy Hb* is the same as in photolyzed Hb*CO and Hb*NO. Although different in intensity, the similarity between the Hb_{II}^* transient absorption bands in Hb*CO and deoxy Hb* indicates that photophysical decay in both occurs by means of similar pathways.

Femtosecond transient absorption spectra and sub-picosecond (sub-ps) time-resolved resonance Raman spectra presented here contribute to a new explanation of photolysis and of the photophysical processes that contribute to the rapid electronic relaxation of heme. Transient absorption data presented here identify the short-lived electronic state Hb_I^* as an iron-to-porphyrin ring charge transfer (CT) state. The CT character of Hb_I^* may explain the ultrafast decay of this state, but more importantly the charge transfer event provides a mechanism for photolysis. The mechanism proposed here explains the origin of the ultrafast intersystem crossing that has been proposed to cause photolysis (Greene et al., 1978; Waleh and Loew, 1982). The transition from the $\pi-\pi^*$ state ^1Q to the Hb_I^* charge transfer state has precedence in spin cross-over reactions (Adams and Hendrickson, 1996; Adams et al., 1997; Sorai and Seki, 1974). The CT process provides a driving force for the entropy-driven spin state change. Stabilization occurs in the CT state due to the stability of a high spin d^5 Fe(III) in the CT state. Time-resolved resonance Raman data show that the Hb_{II}^* state consists of a high-spin heme iron, which is significantly displaced out of the heme plane in both Hb*CO and Hb*NO, even at 1 ps after photolysis. These data lead to the hypothesis that the difference between excited state dynamics of ligated and unligated hemes is not principally due to heme geometry or iron spin multiplicity, but is likely due to differences in the iron d-electron configuration that depend on the different energies available following back electron transfer.

METHODS

The Raman data described in this paper were obtained using a two-color TRRR spectrometer with 700-fs Raman excitation pulse at 435 nm and a 100-fs pump pulse at 570 nm. The apparatus has been described in detail elsewhere (Petrich et al., 1987). The Raman beam, which is in resonance with the Soret band of hemoglobin at 435 nm, was generated by using the frequency-doubled output of a chain of three amplifiers using laser dye LDS867. The frequency bandwidth of the Raman beam was set by a 6-Å bandpass filter centered at 870 nm. The amplifiers using laser dye LDS867 were pumped by the output of a frequency-doubled injection-seeded YAG laser at 30 Hz. After frequency doubling to 435 nm using a KDP crystal, the bandwidth of the Raman probe pulse was 25 cm^{-1} and the pulse duration was 700 fs with energies of 500 nJ/pulse. A bandpass filter with a sharp cutoff below 437 nm was used as a Rayleigh filter for the Stokes Raman spectra in the low frequency region.

The pump pulse used in these experiments was a 100-fs pulse centered at 570 nm with an energy of 50 μJ/pulse. The pulses were made collinear using a dichroic mirror which had a high reflectivity at 570 nm at an angle of 45° and a high transmissivity at 435 nm. Experiments were done in which the pump intensity was reduced by one-half and one-quarter and the signal size decreased proportionally with no detectable change in form. The extent of photolysis (~50%) and signal linearity indicate that the pump pulse intensities are about twice those used extensively in femtosecond transient absorption measurements. The timing between pump and Raman scattering pulses was determined using a parallel transient absorption experiment in which the photolysis of a sample HbCO or deoxy Hb was monitored.

Typical Raman samples consisted of HbNO, HbCO, or deoxy Hb, which were 200–400 μM in heme. Sample preparation has been described elsewhere (Petrich et al., 1987). Intensity changes were obtained relative to an internal standard of 1M Na_2SO_4 with a peak at 983 cm^{-1}, which could be compared to the largest Raman bands of hemoglobin and myoglobin ν_7 at 674 cm^{-1} and ν_4 at 1355 (1370) cm^{-1} for deoxy and CO species, respectively.

The data analysis procedure used to obtain relative intensities and frequencies as a function of time consists of fitting the observed Raman bands to a Lorentzian model,

$$L_S(\omega) = A_0\left[\frac{A_S\Phi\Gamma}{\pi[\Gamma^2 + (\omega - \omega_0 - \omega_S)^2]} + \frac{(1-\Phi)\Gamma}{\pi[\Gamma^2 + (\omega - \omega_0)^2]}\right], \quad (1)$$

which is constrained to have the same center frequency, ω_0, and fwhm, Γ, at all time points. However, the model allows for a time dependence of the relative amplitude, A_S due to photophysical processes and the time dependence of the frequency shift relative to the center frequency, ω_S, for each time delay of the photoproduct Raman band. In Eq. 1, Φ is the photolysis yield and A_0 is the amplitude of the reactant Raman band at equilibrium. A_s is equal to the relative intensity of the photoproduct Raman band because Γ is the same for all time points.

Single-wavelength transient-absorption kinetics were measured and combined to obtain a schematic representation of time-resolved spectra on the picosecond time scale. The time-resolved absorption spectrometer has been described elsewhere (Petrich et al., 1988). In addition to single-wavelength kinetics, we have obtained time-dependent spectra using an EG&G cryogenic charge-coupled device (CCD) detector and a software controller of local origin. For both single-wavelength and CCD-detected spectra, the probe beam was split into a sample probe beam that passed

through the sample and a reference beam that had a parallel trajectory through air. The variations in the probe beam intensity were corrected by taking the ratio of the probe to reference beam. In addition, the intensity of the reference beam was monitored on a shot-to-shot basis and those shots that deviated by more than 60% from the average intensity were not included in signal averaging.

Calculations of absorption spectra and resonance Raman (RR) excitation profiles were done using the program TIMETHERM (Shreve and Mathies, 1995). This program uses the time-correlator formalism to calculate RR excitation profiles at a selected temperature. Calculations of absorption and Raman spectra are greatly facilitated by the measurement of absolute RR cross-sections of deoxy Mb (Bangcharoenpaurpong et al., 1984). The calculation at a given temperature is performed with the intent of modeling the instantaneous Raman spectrum at a given time, and hence a given temperature in a hot molecule. Calculations of nonequilibrium distributions were carried out using the sum-over-states formalism (Myers and Mathies, 1987; Shreve and Mathies, 1995).

RESULTS

Time-resolved resonance Raman measurements

Time-resolved RR spectra comparing HbCO and HbNO are shown in Fig. 1. The 505-cm^{-1} Fe–CO stretching mode (Armstrong et al., 1982; Tsubaki et al., 1982) shows an intensity decrease (negative feature in the difference spectrum) at all three delay times (1, 3, and 10 ps). The intensity changes in this mode serve as an internal calibration of the photolysis yield and the zero time of the pump-probe overlap. In the HbNO ground-state spectra, there is no observable intense Hb–NO stretch or Hb–N–O bending mode. The increase in intensity of two modes at 225 and 304 cm^{-1} in both HbCO and HbNO is an indication that the heme iron has moved out of the heme plane within 1 ps after the photolysis flash (Argade et al., 1984; Findsen et al., 1985; Nagai and Kitagawa, 1980). The equilibrium spectrum of HbNO differs from that of HbCO in the low-frequency region. The feature at $\approx$265 cm^{-1} in the equilibrium HbNO spectrum in Fig. 1 *B* is similar to a feature seen in the equilibrium MbCO spectrum (Choi and Spiro, 1983; Tsubaki et al., 1982; Wells et al., 1991) and the Hb*NO difference spectra bears a resemblance to Mb*CO difference spectra (Franzen et al., 1995a). Using the ν_7 band at 674 cm^{-1} as an internal standard, there is no significant frequency shift or reduction in the intensity of the low-frequency modes in Hb*NO until NO geminate recombination begins to occur on the 10-ps time scale. The justification for use of ν_7 as an internal standard for comparison of the intensities of low frequency modes has been presented in a previous paper (Franzen et al., 1995a).

A comparison of the ν_4 band shift in Hb*CO and Hb*NO is shown in Fig. 2. Several experiments have shown a time-dependent frequency shift of the electron density marker mode, ν_4 (observed at 1355 cm^{-1} in deoxy Hb) for photoexcited deoxy Hb*, and photolyzed Hb*CO and Mb*CO within the first few picoseconds after photoexcitation (Franzen et al., 1995b; Li et al., 1992; Petrich et al., 1987). The ν_4 or electron-density marker band is a sensitive

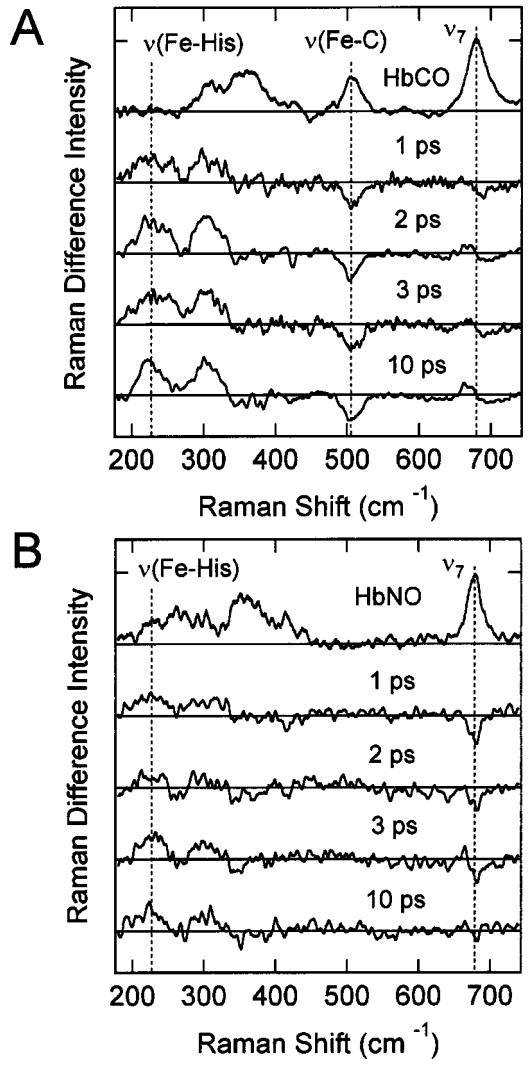

FIGURE 1 Time-resolved RR spectra of the low-frequency region of HbCO and HbNO. (*A*) The top spectrum obtained at a delay of -5 ps is the equilibrium HbCO resonance Raman spectrum. Raman difference spectra Δ(HbCO at τ ps $-$ HbCO at -5 ps) are shown for delay times of 1, 3, and 10ps. (*B*) The top spectrum the equilibrium spectrum of HbNO obtained in the same way as that of HbCO. Raman difference spectra are shown below obtained under identical conditions to those of HbCO at delay times of 1, 2, 3, and 10 ps. The spectra were normalized to the intensity of the ν_7 Raman band.

probe of the electrostatic environment of the heme iron. The ν_4 band shift in Hb*CO due to heme photophysics has a maximum value of $\approx$4 cm^{-1} at 1–2 ps after a photolysis flash, and is significantly smaller than the deoxy Hb* band shift of $>$7 cm^{-1}. The time constant for relaxation of the frequency shifts is $\approx$3–4 ps. As seen in Fig. 2, similar frequency shifts of the ν_4 band are seen in Hb*NO and Hb*CO at the 1, 2, and 10-ps time delays. Although the rapid recombination of the NO ligand makes it difficult to quantify the relaxation of the ν_4 band beyond 1 ps in Hb*NO, it appears based on the 1- and 2-ps time points that

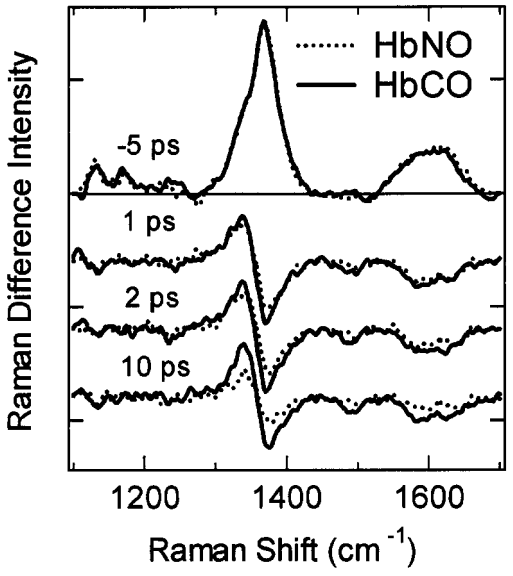

FIGURE 2 Time-resolved resonance Raman spectra of the high frequency region of HbCO and HbNO. The top spectrum in the left panel was obtained at a delay of −5 ps and is the equilibrium HbCO resonance Raman spectrum. Raman difference spectra Δ(HbCO at τ ps − HbCO at −5 ps) are shown for delay times of 1, 2, and 10 ps. The top panel is the equilibrium spectrum of HbCO and HbNO obtained under identical conditions. Raman difference spectra are shown below for HbCO (——) and HbNO(· · · ·) at delay times of 1, 2, and 10 ps. The spectra were normalized to the intensity of the ν_4.

both exhibit similar shifts in frequency of ν_4 during the lifetime of the state.

There is nearly uniform reduction of Raman intensities across the Raman spectrum, which recovers to the original intensity on the same time scale (≈3–4 ps) as the decay of the shifted frequency of the ν_4 mode. The maximum reduction in intensity in time-resolved Raman spectra is ≈30% in deoxy Hb*. Low-frequency Raman bands, such as the ν_7 band and the ν(Fe-His) band of Hb*CO have a similar intensity reduction to that of deoxy Hb*. By contrast, the ν_4 Raman band of Hb*CO shows only about half as large an intensity reduction (i.e., only 15%). The frequency of ν_4 and intensity of ν(Fe-His) on the 3–4-ps time scale indicate that the heme iron is significantly displaced from the heme plane in the Hb^*_{II} state in both Hb*CO and Hb*NO.

The observation of a uniform decrease in the RR scattering intensity with a 3–4-ps lifetime agrees with the observation of a decrease of scattering intensity between 2 and 5 ps observed using 8-ps pulses (Lingle et al., 1991). The results agree further with Raman saturation experiments (Li et al., 1992) in which a reduction in the Stokes scattering intensity is observed and a shift of the ν_4 band occurs in a bottleneck state with a reported lifetime of ~2.0 ± 0.7 ps in hemoglobin. Saturation Raman spectroscopy has also been interpreted elsewhere in terms of a 4-ps lifetime for IVR in heme (Alden et al., 1992, Schneebeck et al., 1993). The intensity of the Raman beam used in the experiments reported here was too low to allow ground-state equilibrium anti-Stokes Raman bands to be observed.

Transient absorption spectra

Transient absorption spectra were studied by two methods. First, kinetics at ten wavelengths were obtained for both deoxy Hb* and Hb*CO. This method is most appropriate for obtaining the time course at any given wavelength. Time-dependent spectra were obtained using a CCD detector, which is most appropriate for obtaining the spectrum at any given time. It is difficult to obtain a good ratio of the probe and reference beam over a wide spectral range, and, hence, the kinetics are slightly poorer with the CCD than with a diode.

In previous studies using single-wavelength kinetics, a shifted Soret feature with a 2.5–3.2-ps lifetime was observed at 450 nm, shifted by 15 nm with respect to the ground state Soret band of deoxy Hb (435 nm). The feature was associated with the state called Hb^*_{II}. The proximity of Hb^*_{II} band to the ground state Soret band leads to the question of whether this feature is attributable to an excited state or a hot ground state. The time-dependent shift in the Soret absorption spectrum was studied to distinguish these two scenarios.

The Soret band shifts were analyzed by two different methods (Lambright et al., 1991). 1) The peak region was fit to a polynomial to interpolate the 1-nm spectral resolution of the CCD. The maximum of the polynomial was found to accurately determine the time dependence of the band shift. 2) Singular value decomposition (SVD) was used to determine whether components that resemble the first derivative (a band shift) can be identified. The time course of such an SVD spectral component gives the time dependence of the band shift.

The use of SVD in the analysis of CO recombination kinetics and Soret band shifts on the nanosecond to microsecond time scale in hemoglobin has been described (Hofrichter et al., 1983). Since an earlier study on Hb^*_{II}, (Petrich et al., 1988), there have been a number of papers that have analyzed Soret band shifts in Mb*CO due to conformational changes on a range of time scales from picosecond to microsecond using SVD (Ansari et al., 1992; Lambright et al., 1991).

Singular-value decomposition is useful when combined with a kinetic model because it allows efficient fitting of a large data set to extract the spectra of kinetic components. The SVD procedure reduces the data matrix A(columns, rows) = A(λ, t) to n orthogonal basis components,

$$A(\lambda, t) = \mathbf{UWV}^T. \quad (2)$$

The columns of **U** are basis spectra as a function of λ. Associated with each column of **U** is a weight or eigenvalue

in the diagonal matrix **W** and a time course in a row of $\mathbf{V}^{T}$. Only the first few spectra typically need to be considered because the weight in **W** diminishes rapidly for higher components. Those components whose weight in the **W** eigenvalue matrix are greater than the noise are retained in the fitting.

To extract information from the data, a selected number of these time courses are fit simultaneously to sums of exponentials or other appropriate kinetic model functions. The first N components of V_n^T can be simultaneously fit to a sum of M exponentials,

$$V_n^T(t) = \sum_{m=1}^{M} C_{nm} e^{-k_m t}, \tag{3}$$

or, more appropriately, exponentials with pulse deconvolution (Naganuma et al., 1989; Yamaguchi and Hamaguchi, 1995). (The chirp artifact due to the second-order cross-phase modulation of the femtosecond probe pulse [Naganuma et al., 1989; Yamaguchi and Hamaguchi, 1995] produces non-negligible autocorrelation values for basis spectra for $n = 3$–5 [i.e., there are spectral features not due to the photoexcitation of myoglobin, but rather cross-phase modulation of the pump and probe in the solvent at zero time]. The first-order dispersion was corrected by a pair of prisms resulting in a second-order [parabolic] dispersion in the sample. The minimum in the parabolic dispersion was centered at 450 nm and the chirp was less than 100 fs over the spectral range 430–470 nm. The second-order [parabolic] chirp over the entire spectral range from 400 to 500 nm was 800 fs. The time courses, which correspond to these basis spectra, are oscillatory and decay to within <1 ps, indicating that these chirp artifacts do not contribute to the kinetics of Hb_{II}^*. From the absence of oscillatory features in components $n = 1$–2, it appears that the SVD components $n = 3$–5 have little or no spectral signature of Hb_{II}^*, although small distortions are possible due to the short lifetime of this electronic state.) The fitting procedure used in Eq. 3 invokes nonlinear simplex fitting for the exponential parameters k_m, and linear least squares fitting for the coefficients C_{nm}. From the matrix of coefficients, C_{nm}, we generate the spectrum $S_m(\lambda)$ of each of the m exponential components,

$$S_m(\lambda) = \sum_{n=1}^{N} C_{nm} U_n(\lambda). \tag{4}$$

The U basis spectra for photoexcited Hb*CO and deoxy Hb* are shown in Figs. 3 *A* and 2 *B*. The U_1 component of the deoxy Hb* species resembles the first derivative of the Soret absorption spectrum, which indicates the Soret band shift. The U_2 component has the broad absorption band of Hb_I^* peaked near 478 nm. The U_1 component of Hb*CO consists of an increase in absorbance at 418 nm, a shift in the Hb*CO Soret band, and an absorbance increase between

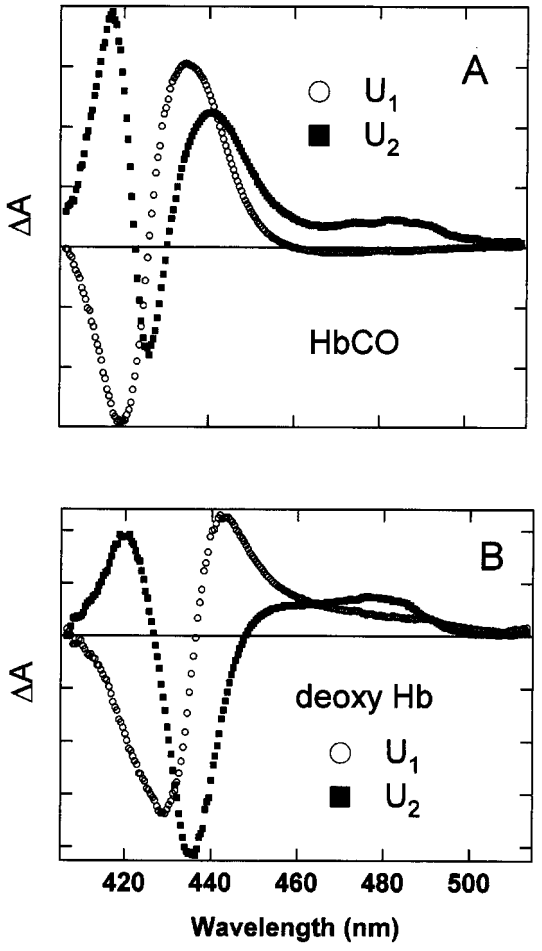

FIGURE 3 Basis spectra from singular value decomposition of time-dependent spectra of Hb*CO and deoxy Hb*. The data set extended from 400 to 500 nm with time delays every 100 fs from 0 to 9 ps after the excitation flash. (*A*) The U_1 and U_2 components from SVD analysis of Hb*CO. (*B*) The first two U components from the SVD analysis of deoxy Hb*. The eigenvalues of the U_3 and higher components were less than 1% of those of U1 and were not considered in the analysis.

460 and 500 nm that has been associated with Hb_I^* in previous work (Petrich et al., 1988). The time courses, V_n^T, which correspond to each of the U_n basis spectra, are shown in Figs. 4 *A* and 3 *B* for Hb*CO and deoxy Hb*, respectively. Although a biexponential model gives an inferior fit to these data, the parameters that correspond to the fit are similar to those obtained from single-wavelength data (see Table 1). Fits to the data using a three-exponential sequential model represent the data well (Eq. 3) and are shown as solid lines. Rate constants (k_m) and coefficients (C_{nm}) are given in Table 2. The time constants of the decay of the shifted Soret band in the three-exponential fit are 1.4 and 5.5 ps instead of a single component of 2.5–3.2 ps observed in the biexponential fit. The spectra that correspond to each of the exponential decays (Eq. 4) are shown in Figs. 5 *A* and 4 *B* for HbCO and deoxy Hb, respectively. In both deoxy

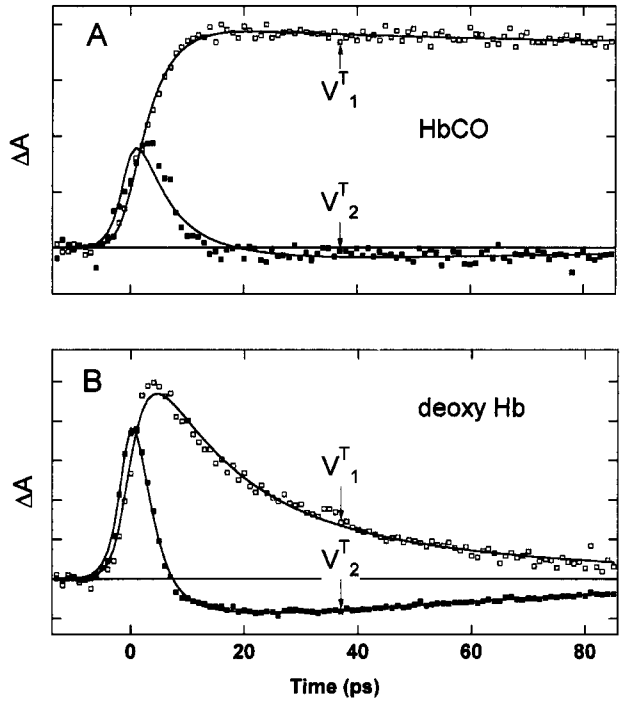

FIGURE 4 Basis time courses for Hb*CO and deoxy Hb*. The time courses $V^T_{1,2}$ correspond to the first two basis spectra $U_{1,2}$. The solid lines drawn through the data are fits to a sum of three exponentials (Eqn. 2) including pulse deconvolution for the 80-fs cross-correlation time. (*A*) The $V^T_{1,2}$ components for Hb*CO are shown. The data show an overall net change from ligated HbCO to an unligated spectrum. There is negligible CO recombination on the 9-ps time scale shown. (*B*) The $V^T_{1,2}$ components for deoxy Hb* are shown. The overall decay corresponds to the relaxation of deoxy heme to the ground state.

Hb* and Hb*CO, the 250-fs exponential component has a broad absorption with peak at 478 nm that has been attributed to Hb^*_I. There is an increase in absorbance at 418 nm in Hb*CO that is not seen in deoxy Hb*. The 1.4-ps components of both deoxy Hb* and Hb*CO are shifted Soret bands. The 5.5-ps component of Hb*CO has roughly the same shape as the 5.5-ps component in deoxy Hb*; however, it is shifted so that the zero crossing is at 430 nm (rather than near the peak of the deoxy Soret band at 435 nm). Whether fit to two or three exponentials, the amplitude of the shifted features in the 1.4 and 5.5-ps components is five times smaller in Hb*CO than in deoxy Hb*, which is in agreement with a previous assignment (Petrich et al., 1988).

SVD was applied to single-wavelength data sets consisting of kinetics obtained at 10 different wavelengths as well. As above, two basis spectra (and time courses) adequately

TABLE 1 Parameters for simultaneous fit of singular value decomposition components to a biexponential model

Component	430 fs	3.1 ps	Baseline
Error	(±110 fs)	(±0.4 ps)	
HbCO			
V_1	−0.163	0.017	0.148
V_2	0.154	0.011	−0.008
Deoxy Hb			
V_1	0.006	0.170	—
V_2	0.375	−0.077	—

TABLE 2 Parameters for simultaneous fit of singular value decomposition components to a three-exponential model

Component	250 fs	1.4 ps	5.5 ps	Baseline
Error	(±80 fs)	(±0.2 ps)	(±0.6 ps)	
HbCO				
V_1	−0.160	0.163	0.001	0.144
V_2	0.113	−0.019	0.052	0.000
Deoxy Hb				
V_1	−0.139	0.062	0.173	—
V_2	0.394	−0.057	0.054	—

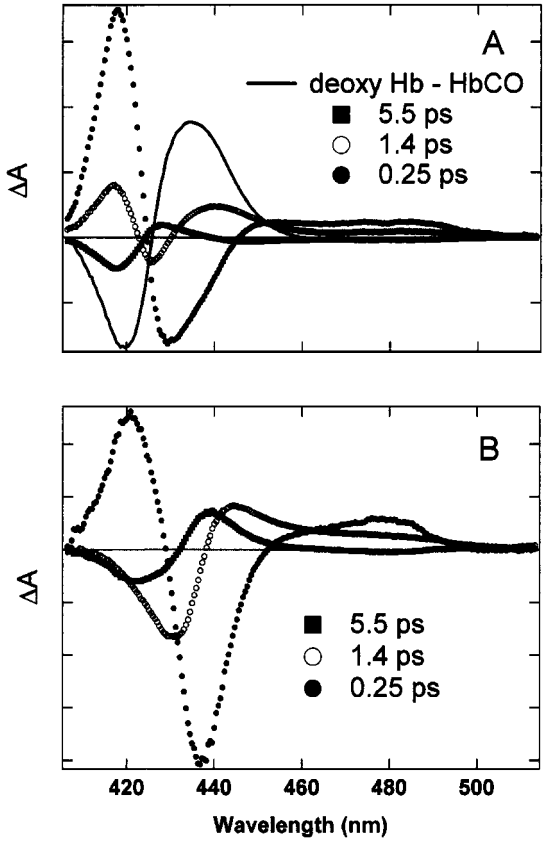

FIGURE 5 Spectral components of the three exponentials required to fit the Hb*CO and deoxy Hb* data. The spectra were calculated from a linear combination of the basis spectra as described by Eq. 3. (*A*) Spectral components for the Hb*CO data. The solid line represents the difference between the pre-flash HbCO equilibrium spectrum and the spectrum at 9 ps, which is essentially a deoxy Mb spectrum. The remaining components represent relaxation processes that occur with single exponential time constants indicated. (*B*) Spectral components for deoxy Hb*. Relaxation to the deoxy Hb* ground state is essentially complete by 9 ps. Therefore, the three components indicated represent phases of relaxation toward the deoxy Hb ground state.

represented the entire data set. The SVD time courses of 10 kinetic traces fit simultaneously were well fit by a biexponential model for deoxy Hb*, and a biexponential including a baseline for Hb*CO (data not shown) confirm previous results (Petrich et al., 1988). A component that decays with a time constant ≈300 ± 70 fs was assigned to Hb_I^*, and second component that decays with a time constant ≈2.9 ± 0.4 ps was designated Hb_{II}^*. The Hb_I^* component has λ_{max} at 478 nm and is observed with approximately the same relative magnitude in both Hb*CO and deoxy Hb*. By contrast, the magnitude of the Hb_{II}^* component, with λ_{max} at 450 nm, depends on the ligation state of the heme. The magnitude of the component due to Hb_{II}^* in Hb*CO is at least a factor of five smaller than that in deoxy Hb*, which is in agreement with the spectra presented above and with previous measurements (Petrich et al., 1988).

We applied a polynomial fit to the peak region of the spectral data for the Soret band in both deoxy Hb* and Hb*CO. The position of the peak, along with a fit to an exponential with a lifetime of 2.2 ps are shown in Fig. 6, *A* and *B*, for Hb*CO and deoxy Hb*, respectively. On time scales longer than 10 ps, there is a residual shift of ≈5 nm in Hb*CO to lower energy than deoxy Hb* that arises from conformational strain. This shift is seen in Soret band shifts on the ≈50-ns and ≈1-μs time scale associated with protein structural relaxations before the R→T transition, which occurs on the 20-μs time scale (Hofrichter et al., 1983).

Calculation of resonance Raman and absorption spectra

Time-dependent spectral shifts appear in both the transient Soret band and in the position of the ν_4 band in the TRRR

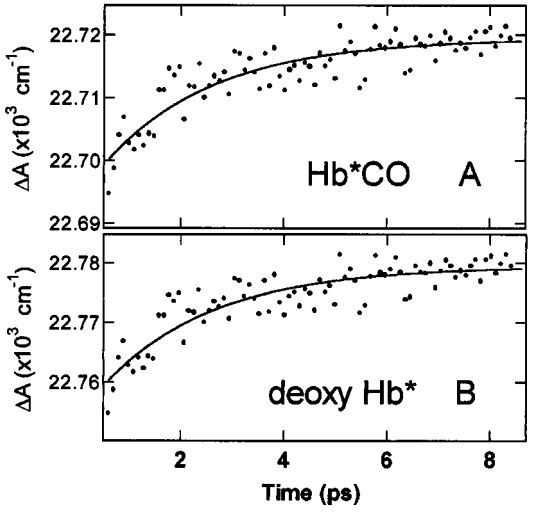

FIGURE 6 Peak position of the deoxy Hb* Soret band in photoexcited HbCO and deoxy Hb. The equilibrium position of the deoxy Hb Soret band is 22,980 cm^{-1}. (*A*) The shift of the photolyzed Hb*CO Soret band is shown along with a fit to a single exponential component with a 2.2-ps lifetime. (*B*) The shift of the photoexcited deoxy Hb* Soret band is shown.

spectrum. There is also a reduction in intensity in the TRRR spectrum that decays with a time constant of ≈3 ps. Calculations were performed to test whether picosecond time dependence of the peak position of the Soret band and changes in intensity of the Raman bands arise from vibrational relaxation and cooling. The five strongest Franck–Condon active modes of the ground state deoxy Soret band were used for these model calculations (Bangcharoenpaurpong et al., 1984). The five modes used in the calculation are 150, 216, 370, 674, and 1355 cm^{-1} whose electron–phonon coupling constants, *S*, of 0.04–0.09, 0.06–0.16, 0.02, 0.035, and 0.058, respectively, have been determined by absolute resonance Raman cross-section measurements (Bangcharoenpaurpong et al., 1984). The electron–phonon coupling $S = \Delta^2/2$. The nuclear displacement in the excited state, Δ, is given in units of the root-mean-square displacement of the zero point motion [Myers and Mathies, 1987]. Studies of spectral broadening in deoxy Mb have shown that homogeneous [300 cm^{-1}] and inhomogeneous [400 cm^{-1}] broadening is required to fit the Soret absorption lineshape (Srajer and Champion, 1991). These values were used for the model calculations.

The calculations as a function of temperature are intended to represent the instantaneous spectrum of the heme molecule at a given time during the cooling process. Calculations of difference absorption spectra and $\Delta A(T_{high} - T_{low})$ spectra show spectral broadening of the Soret band with increasing temperature (calculation not shown). The magnitude of $\Delta A(T_{high} - T_{low})$ decreases as the inhomogeneous broadening increases and is quite small for the Soret band with an inhomogeneous linewidth of ≈400 cm^{-1}. It is possible that the change in broadening could appear as a shift in the low energy lobe of a broadened absorption spectrum. However, even for an initial temperature of 1200 K, which corresponds to a situation where all of the energy of an absorbed photon remains in the Franck–Condon active modes of the absorptive transition, the largest possible apparent shift in the lobe of the Soret band is ≈100 cm^{-1}. This shift is too small by a factor of five when compared to the experimental results for deoxy Hb* (Fig. 6). The asymmetric shape of the observed spectra in Fig. 5 does not appear to be that of an equilibrated hot Soret absorption band. Calculations that assume a nonthermalized distribution using a sum-over-states formalism (Shreve and Mathies, 1995) can produce a shifted (rather than broadened) Soret band, however large values of the nuclear displacement in ν_4 ($\Delta > 1$) must be used. These calculations suggest a nonequilibrium distribution in which ν_4 is a bottleneck consistent with data obtained elsewhere (Kholodenko et al., 2000; Schneebeck et al. 1993).

The relative intensities in the time-resolved resonance Raman data indicate that the heme is not simply hot, but energy is trapped in certain modes on the picosecond time scale. Figure 7 shows a simulated 300-K RR spectrum for

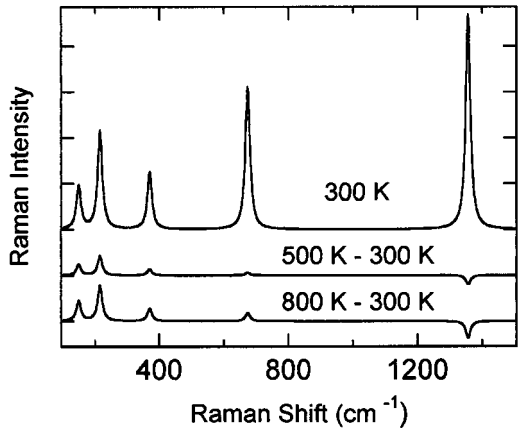

FIGURE 7 Calculated RR spectra for excitation at 435 nm as a function of temperature. The RR spectrum, calculated using the 5-mode model and parameters in the text, is shown, for a temperature of 300 K. Raman difference intensities for spectra at 300 K subtracted from calculated Raman spectra at 500 K and 800 K, respectively, are shown as the bottom two traces in the Figure. Similar results are obtained for other excitation wavelengths.

excitation at 435 nm (at the peak of the deoxy Hb Soret band) based on the same five-mode model used for the absorption spectrum calculation. Lorentzian lines with 17-cm^{-1} linewidths were used to simulate the actual Raman spectrum. A comparison of RR temperature difference spectra at 500–300 K and 800–300 K is shown in Fig. 7, *B* and *C*, respectively. Although only the Stokes Raman spectra are presented in Fig. 7, the magnitude of the intensity changes at various temperatures is nearly the same on the anti-Stokes and Stokes side. However, the intensity changes have the opposite trend as a function of mode frequency. At higher temperatures, the relative intensity of the high-frequency modes increases for anti-Stokes spectra, whereas it decreases for Stokes spectra. The calculated Stokes RR intensities of all of the modes below 1000 cm^{-1} increase as the temperature is increased in the ground state. By contrast, the experimental observations indicate that the intensities of all modes decrease uniformly in the excited state (Li et al., 1992; Lingle et al., 1991). The relative intensities are indicative of a relatively larger degree of energy trapped in high-frequency Franck—Condon-active modes ν_7 and ν_4 (Scheebeck et al., 1993). The question remains as to whether the shift in ν_4 band seen in time-resolved resonance Raman spectra arises from this nonequilibrium distribution or from population of an excited state. In the following, it is shown that the iron is trapped in a ligand field state on the time scale of these relaxation processes. This state has the appearance of the ground state if the porphyrin ring is considered, (Kholodenko et al., 2000) but still has a non-equilibrium population of iron d-states.

DISCUSSION

There are three experimental indicators of the photophysical state of the heme relax on the 3–4-ps time scale: the Soret absorption band shift, RR intensity reductions, and the ν_4 mode frequency shift. There are two possible sequential schemes that explain these features. In sequential path 1, the path proceeds from $^1Q \rightarrow Hb_I^* \rightarrow Hb$, where Hb is the vibrationally hot ground state (Kholodenko et al., 2000). The return to the heme ground state occurs with ≈300-fs decay time of the Hb_I^* state (shown by the dashed arrow in Fig. 8). In this pathway, the ≈3–4-ps component is the result of a hot ground state. In sequential scheme 2, $^1Q \rightarrow Hb_I^* \rightarrow Hb_{II}^* \rightarrow Hb$, the ≈3–4-ps phase is a heme excited state that may also be hot (Alden et al., 1992; Li et al., 1992; Schneebeck et al., 1993). A further possibility consists of a branched or parallel pathway involving decay from Hb_I^* to both Hb and Hb_{II}^* as shown in Fig. 8 (Petrich et al., 1988). The following discussion supports the hypothesis that Hb_I^* is a charge transfer state and Hb_{II}^* consists of an excited iron d-electron configuration formed by a sequential pathway of scheme 2. This model resolves the contradiction between the numerous interpretations of the experimental data. (Kholodenko et al., 2000; Lim et al., 1996; Schneebeck et al., 1993; Li et al., 1992; Petrich et al., 1988) The apparent difference between deoxy and CO heme in the transient absorption spectra is due to a difference in the d-orbital populations of the iron during picosecond relaxation during the kinetic phase associated with Hb_{II}^*. This may be viewed as a ground state with incomplete intramolecular vibrational relaxation in the porphyrin ring. However, the difference between deoxy and CO spectra is explained by differences in the iron d-states during the picosecond relaxation.

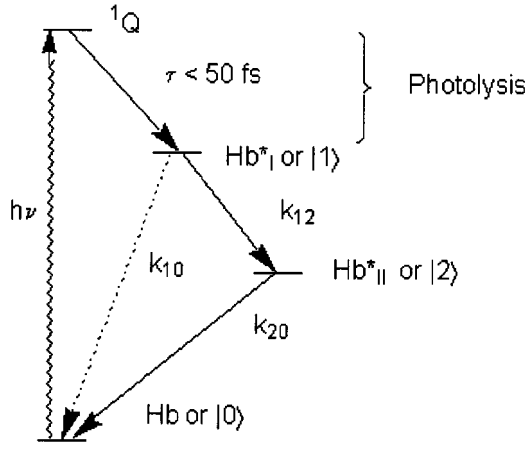

FIGURE 8 Kinetic scheme for heme photophysical decay. Photoexcitation to the ^1Q state is shown by the wavy arrow. Photolysis occurs on the time scale of the rapid deactivation of ^1Q to the Hb_I^* state. The thick arrow represents the possibility that an additional state is populated that cannot be experimentally observed. The decay from Hb_I^* back to the ground state can occur directly (*dashed arrow*) or by way of the Hb_{II}^* state (*solid arrows*).

Metalloporphyrin-excited states and valence tautomerism

Although the electronic relaxations of heme are extremely rapid, certain features in the transient absorption and Raman spectra bear a resemblance to spectra of metalloporphyrins that relax by electronic processes that are orders of magnitude slower than heme. Specifically, the 450-nm absorption band in Hb^*_{II} can be compared to excited-state absorption bands of a large number of metalloporphyrins that appear at slightly lower energy than the Soret band. Likewise, the transient reduction in the frequency of the ν_4 oxidation state marker band in Hb^*_{II} can also be compared to similar shifts in excited states of other metalloporphyrins (Kreszowski et al., 1994). The states that have nanosecond lifetimes are clearly S_1 porphyrin states ($e_g(\pi^*)$ states) as shown by the transient Raman spectra of chlorophylls (Nishizawa et al., 1989). In closed shell metalloporphyrins, these states decay to the T_1 porphyrin triplet states on the nanosecond to microsecond time scale (Gentemann et al., 1993), Closed shell Ni appears to decay via d–d excited states that have transient open shell character (Findsen et al., 1988; Kim and Holten, 1983). For Ni-porphyrins, both the transient Q-band spectrum and the ν_4 Raman mode are shifted to lower energy during the lifetime of the excited state. If an open shell metal, such as ruthenium (Ru) is the central metal in a porphyrin-excited state, decay occurs by a charge transfer mechanism (Levine and Holten, 1988; Rodriguez et al., 1988) that also exhibits a shift in ν_4 to lower energy during the excited-state lifetime (Vitols et al., 1995). However, excited-state relaxation in Ru porphyrin is much slower than in heme. The 4d-orbital energies are more widely separated in energy by the Ru ligand field and are more weakly coupled to the porphyrin π system than are the 3d orbitals of iron, thus reducing the electronic coupling in charge transfer decay channels. Analogy with Ru porphyrin photophysics suggests that Hb^*_I may be a [d, π^*] CT state. In contrast to Ru porphyrins, the [d, π^*] CT (Hb^*_I) state in heme lies below the [π, π^*] state in energy. Moreover, coupling between the CT state and ligand field states of the metal is significantly stronger in heme than in Ru porphyrins, hence leading to the extremely rapid deexcitation of the heme macrocycle. CT states have been investigated as the pathway for deactivation of Co porphyrins based on the idea that a $Co(I)P^+$-excited state is formed from excitation of Co(II)P (Tait et al., 1984). However, more recent studies have shown that this is not the case, indicating possibly the $Co(III)P^-$ is formed instead (Loppnow et al., 1993). The driving force for the spin transitions in these metalloporphyrins is likely similar to that observed in valence tautomerism in cobalt complexes (Adams et al., 1997). The large entropic contribution to the coupling of charge transfer to spin-state change is due to both the increase in the number of spin states and a contribution of the vibrational entropy (Sorai and Seki, 1974). Although not often noted, both of these factors are present in metalloporhyrins (Ghosh et al., 2000).

There are a large number of excited d–d states in iron porphyrins. Several iron configurations are thermally populated at ambient temperature (Eicher et al., 1976). The model calculations presented in the section, Calculation of Resonance Raman and Absorption Spectra, demonstrate that temperature effects of the porphyrin $\pi-\pi^*$ system do not explain the observed spectral intensities and frequency shifts. Instead, we suggest that nonequilibrium population in iron d_π and d_z2 orbitals may mix with the $e_g\pi^*$ LUMO and the $a_{2u}\pi$ HOMO, respectively, thus perturbing heme spectra on the picosecond time scale. These factors may affect the spectra in the Hb^*_{II} state in analogy with other open-shell metalloporphyrins. In the following, we discuss the evidence that the Hb^*_I state is a short-lived CT state based on the precedent of metalloporphyrins. We then turn to the possibility of parallel or sequential decay pathways of Hb^*_I to either the ground state or Hb^*_{II}.

Hb^*_I is the photolytic state: valence tautomerism versus vibronic coupling mechanisms

The $^1Q \rightarrow Hb^*_I$ transition is the first process observed after photoexcitation or photolysis. The similarity of the Hb^*_I absorption band between 460 and 500 nm for both unligated and ligated forms of Hb* suggests that Hb^*_I is the same electronic state in both ligated and unligated forms of Hb*. Because there is no evidence for ultrafast return to the ground state, and the fluorescence yield of heme is extremely low, (Adar et al., 1976) we conclude that the quantum yield of Hb^*_I is nearly one in both Hb*CO and deoxy Hb*. The broad spectral features of Hb^*_I in the near-infrared region, (Lim et al., 1996) bleaching of the Soret and appearance of a small band at 478 nm (see Figs. 3 and 5) are consistent with formation of a porphyrin ring anion (Closs and Closs, 1963; Gentemann et al., 1993). The spectra do not resemble a ring cation (Dolphin and Felton, 1974), nor are they consistent with a triplet state.

There are several problems with a hypothesis that Hb^*_I is a $^3[\pi, \pi^*]$ porphyrin triplet state, ^3Q. Such a state would require an ultrafast intersystem crossing, and it is also doubtful that the spin–orbit coupling alone is sufficiently strong to account for such a mechanism. The change of spin from $S = 0$ to $S = 1$ or $S = 2$ coupled with an ultrafast CT process implies a transition matrix element $\langle ^1Q|H|Hb^*_I\rangle$, where H is a hamiltonian that may include spin–orbit, vibronic, and exchange terms. The symmetry of Hb^*_I and the ^1Q [π, π^*] excited state (^1E in C_{4v}) are related such that the direct product of $\Gamma(^1Q)\Gamma(R_z)\Gamma(Hb^*_I)$ is A_1. We consider only R_z (and not R_x or R_y) because the orbital angular momentum of the electron in the ^1Q state is in the x, y plane. Mixing of ^1Q with $^{3,5}Q$ is allowed because both states have E symmetry and the EE direct product contains the irreducible representation of the spin–orbit coupling operator, A_2. How-

ever, because photolysis occurs during or before the formation of Hb_I^*, this hypothesis would almost certainly require the $^3[\pi, \pi^*]$ porphyrin triplet state to be the photolytic state. Because this state involves no change in d-orbital occupancy, this seems unlikely.

In Hb*CO, the $d_{yz} \rightarrow a_{1u}, a_{2u}$ transition results in an electronic configuration $[(d_{xy})^2(d_{xz}, d_{yz})^3(d_{x^2x^2-y^2})^0(d_{z^2})^0(a_{1u}, a_{2u})^4(e_g^*)^1]$ producing a ring anion with the symmetry of the direct product $EE = A_1 + A_2 + B_1 + B_2$. If this charge transfer were not coupled to a change in spin state, vibronic coupling would be required. No vibronic coupling needs to be invoked if a valence tautomeric (VT) spin change involving $d_{xz,}d_{yz} \rightarrow d_{z^2}$ or $d_{xz,}d_{yz} \rightarrow d_{x^2-y^2}$ preserves the excited state E symmetry. The Hb_I^* is either $[(d_{xz})^1(d_{xy})^2(d_{yz})^1(d_{x^2-y^2})^0(d_{x^2})^1(a_{1u}, a_{2u})^4(e_g^*)^1]$ or $[(d_{xz})^1(d_{xy})^2(d_{yz})^1(d_{x^2-y^2})^1(d_{x^2})^0(a_{1u}, a_{2u})^4(e_g^*)^1]$.

A porphyrin cation would be formed by a ring-to-iron CT $[\pi^*, d]$ transition. The two $[\pi^*, d]$ processes, $e_g^* \rightarrow d_{z^2}$ and $e_g^* \rightarrow d_{x^2-y^2}$) are both energetically impossible. Both of these CT transitions require changes in state symmetry that requires vibronic coupling. The $e_g^* \rightarrow d_{z^2}$ transition would give a $[(d_{xy})^2(d_{xz}, d_{yz})^4(d_{z^2})^1(d_{x^2-y^2})^0(d_{x^2})^0(a_{1u}, a_{2u})^3(e_g^*)^0]$ configuration, which has A_1 or A_2 symmetry in C_{4v} and a ring cation. The operator responsible for mixing these states with the $E\pi-\pi^*$ excited-state configuration would have to be a vibronic coupling operator $\partial/\partial Q$ with A_2 symmetry. Strong vibronic coupling is conceivable for the charge transfer transition that forms Hb_I^* because heme-doming mode and iron—histidine-stretching modes are two modes of A_2 symmetry that are strongly and coherently excited after photolysis, as demonstrated by femtosecond transient absorption spectroscopy of deoxy and Hb*NO (Zhu et al., 1996).

In VT, the free energy required for the transition is derived primarily from the entropy change. The increase in the entropy arises from both the spin state change and the increase in the number of low frequency modes. The appearance of low frequency Raman active modes in the deoxy Hb* spectra is consistent with this type of mechanism.

For deoxy Hb*, the $[\pi, \pi^*]$ electronic configuration is $[(d_{xz})^2(d_{xy})^1(d_{yz})^1(d_{x^2})^1(d_{x^2-y^2})^1(a_{1u}, a_{2u})^3(e_g^*)^1]$, which is a ^5E configuration (Eaton et al., 1978). Here, VT cannot occur because the heme is already high spin. However, the $[d, \pi]$ transition $d_{z^2} \rightarrow a_{1u}, a_{2u}$ is symmetry allowed. One consequence of the CT model is that the electronic configuration of Hb_I^* $[(d_{xz})^2(d_{xy})^1(d_{yz})^1(d_{z^2})^0(d_{x^2-y^2})^1(a_{1u}, a_{2u})^4(e_g^*)^1]$ is the same for both deoxy Hb* and Hb*CO, provided that the $d_{yz} \rightarrow d_{x^2-y^2}$ transition occurs in Hb*CO. The hypothesis that VT occurs in Hb*CO does exclude vibronic coupling to axial out-of-plane modes such as the iron–histidine stretch that can promote the CT process in both Hb*CO and deoxy Hb*. Furthermore, a spin rearrangement to obtain a common configuration of $[(d_{xz})^1(d_{xy})^1(d_{yz})^1(d_{z^2})^1(d_{x^2-y^2})^1(a_{1u}, a_{2u})^4(e_g^*)^1]$ for both Hb*CO and deoxy Hb* will result in a reduction of electron–electron repulsion, which is consistent with Hund's rule. This hypothesis provides an explanation for a common intermediate for Hb*CO and deoxy Hb* consistent with the spectroscopic data (Figs. 3 and 5) and a mechanism for CO photolysis.

The hypothesis that Hb_I^* is a CT state suggests a mechanism for photolysis that has not been considered previously. Earlier proposals have suggested electron promotion from $d_\pi \rightarrow d_{z^2}$ coupled to simultaneous deactivation of the $^1Q\pi^*$ state to the π ground state as a mechanism for photolysis of CO (Waleh and Loew, 1982; Zerner et al., 1966). Formation of Fe(III) by charge transfer has also been mentioned as a mechanism for CO photolysis, however this hypothesis was not developed for lack of experimental data (Vogler and Kunkely, 1976). The data presented here and other recent data support the hypothesis that Hb_I^* is a CT state. It follows that photolysis in Hb*CO may occur due to formation of an intermediate spin CT state. For Hb*CO and Hb*NO, the $d_\pi \rightarrow a_{1u}, a_{2u}$ CT state results in destabilization of the π-backbonding interaction between iron and the ligand.[5] The destabilization of the Fe–CO bond is effected by removal of bonding electrons from the d_π orbitals (reduced π-backbonding). As the Fe–CO bond length increases, the energy of d_{z^2} orbital decreases due to the weakened ligand field. In a rapid subsequent step, a second electron promotion occurs on the iron atom from the d_{xz} orbital to d_{z^2}. This step is promoted by stability of a half-filled shell for d^5 Fe(III), which has an electronic configuration of $[(d_{xz})^1(d_{xy})^1(d_{yz})^1(d_{z^2})^1(d_{x^2-y^2})^1(a_{1u}, a_{2u})^4(e_g^*)^1]$. The VT mechanism proposed here provides an explanation for the rapid spin state change that must precede photolysis. The mechanism works for Hb^*O_2 as well. The charge transfer $d_{z^2} \rightarrow a_{1u}, a_{2u}$ is symmetry allowed similar to the CT proposed in deoxy Hb* and leads to destabilization of the π-backbonding interaction between iron and bent O_2.

The sequential decay hypothesis $Hb_I^* \rightarrow Hb_{II}^* \rightarrow Hb$

The hypothesis for a sequential decay pathway for deoxy Hb* builds on data presented here and in a previous study (Petrich et al., 1988). Although the absorbance of the 478-nm Hb_I^* band is nearly the same in Hb*CO and deoxy Hb*, the intensity of the absorption band associated with Hb_{II}^* for Hb*CO is ⅕ as large as the corresponding band in deoxy Hb*. This difference has been interpreted in terms of a sequential path $^1Q \rightarrow Hb_I^* \rightarrow Hb$, where Hb is a hot ground state (Kholodenko et al., 2000) and in terms of the parallel pathway shown in Fig. 8 (Petrich et al., 1988). Parallel and sequential pathways with one intermediate are shown in Fig. 8 with the identifications, $Hb \equiv |0\rangle$, $Hb_I^* \equiv |1\rangle$, and $Hb_{II}^* \equiv |2\rangle$, so that the rate constant for the process $Hb_I^* \rightarrow Hb_{II}^*$ is k_{12}. The experimental rate constant for the decay of Hb_I^* is $k_{obs} = 3.3 \pm 0.8 \times 10^{12}\ s^{-1}$. The same rate constant is observed for the rise time for the state Hb_{II}^* in deoxy Hb*, Hb*CO, and Hb*NO (Petrich et al., 1988) i.e., $k_{12} \approx 3.3 \times 10^{12}\ s^{-1}$. If a parallel decay pathway drains

population from Hb_I^* (i.e., $Hb_I^* \rightarrow Hb_{II}^*$ and $Hb_I^* \rightarrow Hb$), the observed decay rate of Hb_I^* (k_{obs}) is the sum of the rates for the two processes, $k_{obs} = k_{10} + k_{12}$, where k_{10} is the rate constant for $Hb_I^* \rightarrow Hb$. If the parallel kinetic model is applied to explain the difference in the magnitude of Hb_{II}^* in Hb*CO, the observed difference in the magnitude of Hb_{II}^* can be interpreted in terms of yield, $\Phi = k_{12}/(k_{12} + k_{10})$. Assuming that the extinction coefficient of Hb_{II}^* is the same for Hb*CO and deoxy Hb*, and given the smaller magnitude of the 450-nm band in Hb*CO, $\Phi \approx 0.2$, and the ground state Hb is formed with a rate constant $k_{10} \approx 4k_{12}$ in a parallel model. However, as seen in the fits to the data, the decay of Hb_I^* is identical in both deoxy Hb* and Hb*CO. Therefore, $k_{10} < k_{12}/4$ according to the kinetic data (given the estimated experimental error of $\pm 25\%$ in the rate constant k_{obs}). There is a factor of 16 discrepancy between the kinetic model and the relative magnitude of the observed spectra if the parallel model is applied.

The parallel decay pathway hypothesis is based on the idea that the yield of Hb_{II}^* is proportional to the observed ΔA at 450 nm and that the extinction coefficient of Hb_{II}^* at ~450 nm is the same for all species. It is possible that the difference in the transient spectra observed for Hb_{II}^* depends on the differences in temperature between the deoxy Hb*, Hb*CO, and Hb*NO species. Often, differences in temperature are interpreted only in terms of vibrational energy, but in hemes the population of excited iron d–d states may also depend on the effects of temperature during a time-dependent relaxation process (Rodriguez and Holten, 1989). A resolution for the discrepancies in rate and quantum yield discussed above can be found if the nature of Hb_{II}^* (and hence the magnitude of ΔA), which depends on the transient effect of temperature on the population of excited iron d–d states. According to this hypothesis, the sequential pathway $^1Q \rightarrow Hb_I^* \rightarrow Hb_{II}^* \rightarrow Hb$ is used for both Hb*CO and deoxy Hb*. The apparent spectral differences in magnitude of the 450-nm band in the Hb_{II}^* state depends on the population of excited iron d–d states during the lifetime of Hb_{II}^*. It is clear from the time-resolved RR spectra that a similar relaxation is taking place with a 3–4-ps time constant in both Hb*CO and deoxy Hb* (Franzen et al., 1995b).

Hb_{II}^* is a temperature-dependent excited d–d state of heme

Previous studies have shown that Hb_{II}^* is an electronic excited state rather than a hot ground state (Petrich et al., 1988). However, the differences in transient absorption and resonance Raman of deoxy Hb* and Hb*CO suggest that there is an effect of temperature on Hb_{II}^* that was not detected in the early experiments. This effect has also been detected in anti-Stokes RR data and has been interpreted as incomplete IVR on the time scale of Hb_{II}^* (Alden et al., 1992; Lingle et al., 1991; Schneebeck et al., 1993).

The hypothesis that Hb_I^* is a CT state (see "Hb_I^* is the Photolytic State: Valence Tautomerism versus Vibronic Coupling Mechanisms") leads to the idea that formation of Hb_{II}^* from Hb_I^* occurs by means of a back CT process on the ≈300-fs time scale. The ring-to-iron CT transitions are $e_g^* \rightarrow d_{yz}$ and $e_g^* \rightarrow d_{xz}$, which leads to configurations of ^5E symmetry, such as $[(d_{xz})^1(d_{xy})^1(d_{yz})^2(d_{z^2})^1(d_{x^2-2})^1(a_{1u}, a_{2u})^4 \cdot (e_g^*)^0]$ and $[(d_{xz})^2(d_{xy})^1(d_{xz})^1(d_{z^2})^1(d_{x^2-2})^1(a_{1u}, a_{2u})^4(e_g^*)^0]$, respectively. The splitting of the d_π orbitals into d_{xz} and d_{yz} that has been observed in ground state spectra of charge transfer bands in deoxy Hb (Eaton et al., 1978) suggests that the population of these states will depend on the temperature of the heme. The available spectroscopic evidence suggests that the heme is cooling on the same time scale (or even a slightly longer time scale) as the decay of the Hb_{II}^* state (Lim et al., 1996; Mizutani and Kitagawa, 1997). The spectral shifts in the transient absorption spectra and the ν_4 vibrational mode on the ≈3–4-ps time scale are due to time-dependent redistribution of the population of excited iron d–d states in Hb_{II}^* and vibrational energy redistribution. Our description of Hb_{II}^* as a porphyrin ground state porphyrin with an excited iron d-electron configuration is based on the equatorial back-bonding model (Antipas et al., 1978), which states that the change in population of the (d_{xz}, d_{yz}) orbitals affects porphyrin absorption and Raman spectra by means of overlap e_g^* porphyrin orbitals. This model explains why the Soret absorption maximum is affected and ν_4 frequency changes, but the ν(Fe–His) frequency does not change because it is coupled to the porphyrin through the d_{z^2} orbital whose population does not change on the 3–4-ps time scale (Stavrov, 1993).

Ligand recombination does not depend on the yield of Hb_{II}^*

A previous hypothesis for the variable quantum yield of Hb_{II}^* was linked to the observation of variable ligand recombination yields. This hypothesis was based on an empirical connection between the intensity of a transient feature in the Hb_{II}^* absorption spectrum (at 450 nm) and the magnitude of the rapid phase of ligand rebinding kinetics. However, the intensity of the Fe–CO stretching mode measured by TRRR does not recover on the ≈3-ps time scale, providing evidence that CO does not recombine (Franzen et al., 1995b). The TRRR data in Fig. 1 show that neither the intensity nor frequency of the ν(Fe-His) mode is significantly altered in Hb*CO or Hb*NO on the picosecond time scale once it appears after photolysis when this mode is normalized to ν_7 (Franzen et al., 1994). The normalization to ν_7 accounts for the uniform change in intensity of all Raman modes as the Hb_I^* state decays and any other fluctuations in intensity resulting from experimental differences. The iron displacement out of the heme plane is nearly complete during the lifetime of the Hb_{II}^* state, showing that the heme iron position is not responsible for the fast phase

of geminate NO recombination in Hb*NO. These results suggest that the yield of Hb^*_{II} is unity for all ligand photoproducts and (deoxy Hb*) and that the differences in ligand recombination rates arise from an intrinsic difference in reactivity toward intermediate and high spin iron.

CONCLUSION

Examination of both transient absorption and time-resolved RR spectra leads to confirmation of the sequential model for excited state decay. After photoexcitation into the ^1Q state, photolysis occurs in less than 50 fs (Petrich et al., 1988) and depopulation of ^1Q in deoxy hemes occurs on a similar time scale. We propose that Hb^*_I is populated directly from ^1Q by a photoinduced-CT process driven by the vacancy in the a_{1u}, a_{2u} HOMO. In Hb*CO, the entropy change associated with an increase in spin multiplicity and population of low frequency modes drives a process that leads to spin conversion and destabilization of the bound CO ligand. We advance the hypothesis that VT is the mechanism for diatomic ligand photolysis in heme, as opposed to a previously proposed mechanism that involves a build-up of electron density in the d_{z^2} orbital due to spin–orbit interactions between the metal and the decaying ^1Q excited state. This proposal explains the similar intensity of the 478-nm Hb^*_I band in Hb*CO, Hb*NO, Hb^*O_2, and deoxy Hb*. The heme iron is in the Fe(III) oxidation state with a similar spin state ($S = 5/2$) in Hb^*_I for all species. The formation of Hb^*_I leads to rapid photolysis of π-acid ligands CO, NO, and O_2.

Hb^*_{II} has an excited d-electron configuration on the iron and a ground state porphyrin ring configuration formed by a ring-to-iron back transfer from the Hb^*_I CT state. The spectral features in Hb^*_{II} are explained as the result of interactions of the ligand field with the porphyrin ring. The transient population of Jahn–Teller splitting of the d_{xz} and d_{yz} orbitals in Hb^*_{II} gives rise to changes in the electronic properties of the porphyrin consistent with the observed spectra, but that may vary in intensity depending on the excess energy in the Hb^*_{II} state.

The TRRR data for both Hb*CO and Hb*NO show similar frequencies and intensities for the ν(Fe-His) mode at the 1-ps time delay. The data indicate nearly complete heme out-of-plane displacement by the time Hb^*_{II} is formed. The absence of a structural difference between the Hb^*_{II} and the ground state in Hb*NO and Hb*CO means that differences in ligand rebinding rates are intrinsic properties of the ligand–iron potential energy surface rather than differences in transient conformation (iron in-plane versus iron out-of-plane). The sequential model involving the formation and decay of CT states proposed for Hb^*_I and Hb^*_{II} presents a cohesive explanation for the electronic relaxation of the heme probed by the subpicosecond TRRR and transient absorption data available for heme proteins.

The results provide an explanation for the fact that π-acid ligands, CO, NO, and O_2, are photolyzed but σ-donor ligands such as imidazole (histidine), H_2O, or pyridine are not. The first essential step in photolysis is metal-to-ring charge transfer from a d_π iron orbital to the a_{1u}, a_{2u} HOMO on the porphyrin ring. The charge transfer process greatly weakens π-backbonding interactions, but has no effect on σ-donor ligands. The charge transfer mechanism provides a consistent explanation for photolysis in heme proteins.

We are grateful to Dr. A. P. Shreve for the use of computer programs for calculation of absorption and RR spectra and for a critical reading of the manuscript. We thank Drs. M. Vos and J. C. Lambry for assistance with transient absorption experiments.

S. Franzen was the recipient of a European Molecular Biology Organization fellowship that supported the experimental work reported here.

REFERENCES

Adams, D. M., and D. N. Hendrickson. 1996. Pulsed laser photolysis and thermodynamics studies of intramolecule electron transfer in valence tautomeric cobalt o-quinone complexes. *J. Am. Chem. Soc.* 118: 11515–11528.

Adams, D. M., L. Noodleman, and D. N. Hendrickson. 1997. Density functional study of the valence-tautomeric interconversion low-spin [CoIII(SQ)(Cat(phen)] = high spin [$CoII(SQ)_2$(phen)]. *Inorg. Chem.* 36:3966–3984.

Adar, F., M. Gouterman, and S. Aronowitz. 1976. Fluorescence, resonance Raman, and radiationless decay in several hemoproteins. *J. Phys. Chem.* 80:2184–2191.

Ahmed, A. M., B. F. Campbell, D. Caruso, M. R. Chance, M. D. Chavez, S. H. Courtney, J. M. Friedman, I. E. T. Iben, M. R. Ondrias, and M. Yang. 1991. Evidence for proximal control of ligand specificity in hemeproteins: absorption and Raman studies of cryogenically trapped photoproducts of ligand bound myoglobins. *Chem. Phys.* 158:329–351.

Alden, R. G., M. C. Schneebeck, M. R. Ondrias, S. H. Courtney, and J. M. Friedman. 1992. Mode-specific relaxation dynamics of photoexcited Fe(II) protoporphyrin IX in hemoglobin. *J. Raman. Spec.* 23:569–574.

Ansari, A., C. M. Jones, E. R. Henry, J. Hofrichter, and W. A. Eaton. 1992. Conformational relaxation and ligand rebinding in myoglobin. *Science.* 256:1796–1798.

Antipas, A., J. W. Buchler, M. Gouterman, and P. D. Smith. 1978. Porphyrins. 36. Synthesis and optical and electronic properties of some ruthenium and osmium octaethylporphyrins. *J. Am. Chem. Soc.* 100: 3015–3024.

Argade, P. V., M. Sassaroli, D. L. Rousseau, T. Inubushi, M. Ikeda-Saito, and A. Lapidot. 1984. Confirmation of the assignment of the iron-histidine stretching mode in myoglobin. *J. Am. Chem. Soc.* 106: 6593–6596.

Armstrong, R. S., M. J. Irwin, and P. E. Wright. 1982. Soret-excited resonance Raman spectrum of (carbonmonoxy)leghemoglobin: assignment of νFe-CO. *J. Am. Chem. Soc.* 104:626–627.

Baldwin, J. M., and C. Chothia. 1979. Haemoglobin: the structural changes related to ligand binding and its allosteric mechanism. *J. Mol. Biol.* 129:175–220.

Bangcharoenpaurpong, O., K. T. Schomaker, and P. M. Champion. 1984. A resonance Raman investigation of myoglobin and hemoglobin. *J. Am. Chem. Soc.* 106:5688–5698.

Carlson, M. L., R. Regan, R. Elber, H. Li, G. N. Phillips, J. S. Olson, and Q. H. Gibson. 1994. Nitric oxide recombination to double mutants of myoglobin: role of ligand diffusion in a fluctuating heme pocket. *Biochemistry.* 33:10597–10606.

Chance, M. R., S. H. Courtney, M. D. Chavez, M. R. Ondrias, and J. M. Friedman. 1990. O_2 and CO reactions with heme proteins: quantum yields and geminate recombination on picosecond time scales. *Biochemistry.* 29:5537–5545.

Choi, S., and T. G. Spiro. 1983. Out-of-plane deformation modes in the resonance Raman spectra of metalloporphyrins and heme proteins. *J. Am. Chem. Soc.* 105:3683–3692.

Closs, G. L., and L. E. Closs. 1963. Negative ions of porphine metal complexes. *J. Am. Chem. Soc.* 85:818–819.

Cornelius, P. A., R. M. Hochstrasser, and A. W. Steele. 1983. Ultrafast relaxation in picosecond photolysis of nitrosylhemoglobin. *J. Mol. Biol.* 163:119–128.

Dolphin, D., and R. H. Felton. 1974. The biochemical significance of porphyrin π cation radicals. *Acc. Chem. Res.* 7:26–32.

Eaton, W. A., L. K. Hanson, P. J. Stephens, J. C. Sutherland, and J. B. R. Dunn. 1978. Optical spectra of oxy- and deoxyhemoglobin. *J. Am. Chem. Soc.* 100:4991–5003.

Eicher, H., D. Bade, and F. Parak. 1976. Theoretical determination of the electronic structure and the spatial arrangement of ferrous iron in deoxygenated sperm whale myoglobin and human hemoglobin from Mossbauer experiments. *J. Chem. Phys.* 64:1446–1455.

Findsen, E. W., J. M. Friedman, M. R. Ondrias, and S. R. Simon. 1985. Picosecond time-resolved resonance Raman studies of hemoglobin: implications for reactivity. *Science.* 229:661–664.

Findsen, E. W., J. A. Shelnutt, and M. R. Ondrias. 1988. Photodynamics of nickel porphyrins in noncoordinate solvents: characterization of d-d excited states using transient Raman spectroscopy. *J. Phys. Chem.* 92: 307–314.

Franzen, S., B. Bohn, C. Poyart, G. DePillis, S. G. Boxer, and J. L. Martin. 1995a. Functional aspects of ultra-rapid heme doming in hemoglobin, myoglobin and the myoglobin mutant H93G. *J. Biol. Chem.* 270: 1718–1720.

Franzen, S., B. Bohn, C. Poyart, and J. L. Martin. 1995b. Evidence for sub-picosecond heme doming in hemoglobin and myoglobin: a time-resolved resonance Raman comparison of carbonmonoxy and deoxy species. *Biochemistry.* 34:1224–1237.

Franzen, S., J. C. Lambry, B. Bohn, C. Poyart, and J. L. Martin. 1994. Direct evidence for the role of heme doming as the primary event in the cooperative transition of hemoglobin. *Nature Struct. Biol.* 1:230–233.

Gentemann, S., J. Albanexe, R. Garcia-Ferrer, S. Knapp, J. A. Potenza, H. J. Shugar, and D. Holten. 1993. Investigation of the lowest electronic states of osmium(II) tetraoylporphyrins: photophysics of metalloporphyrin (d, π^*) charge transfer states. *J. Am. Chem. Soc.* 116:281–289.

Ghosh, A., T. Wondimagegn, E. Gonzalez, and I. Halvorsen. 2000. Valence tautomerism and macrocycle ruffling in nickel(III) porphyrins. *J. Inorg. Biochem.* 78:79–82.

Gottfried, N. H., and W. Kaiser. 1983. Redistribution of vibrational energy in naphthalene and anthracene studied in liquid solution. *Chem. Phys. Lett.* 101:331–336.

Greene, B. I., R. M. Hochstrasser, R. B. Weisman, and W. A. Eaton. 1978. Spectroscopic studies of oxy- and carbonmonoxyhemoglobin after pulsed optical excitation. *Proc. Natl. Acad. Sci. U.S.A.* 75:5255–5259.

Hartmann, H., S. Zinser, P. Komninos, R. T. Schneider, G. U. Nienhaus, and F. Parak. 1996. X-ray structure determination of a metastable state of carbonmonoxy myoglobin after photodissociation. *Proc. Natl. Acad. Sci. U.S.A.* 93:7013–7016.

Hoffman, B. M., and Q. H. Gibson. 1978. On the photosensitivity of liganded hemoproteins and their metal-substituted analogues. *Proc. Natl. Acad. Sci. U.S.A.* 75:21–25.

Hofrichter, J., J. H. Sommer, E. R. Henry, and W. A. Eaton. 1983. Nanosecond absorption spectroscopy of hemoglobin: elementary processes in kinetic cooperativity. *Proc. Natl. Acad. Sci. U.S.A.* 80: 2235–2239.

Jackson, T. A., M. Lim, and P. A. Anfinrud. 1994. Complex nonexponential relaxation in myoglobin after photodissociation of MbCO: measurement and analysis from 2 ps to 56 μs. *Chem. Phys.* 180:131–140.

Keyes, M. H., M. Falley, and R. Lumry. 1971. Studies of heme proteins. II. Preparation and thermodynamic properties of sperm whale myoglobin. *J. Am. Chem. Soc.* 93:2035–2040.

Kholodenko, Y., M. Volk, E. Gooding, and R. M. Hochstrasser. 2000. Energy dissipation and relaxation processes in deoxy myoglobin after photoexcitation in the Soret region. *Chem. Phys.* 259:71–87.

Kim, D., and D. Holten. 1983. Picosecond measurements on the binding and release of basic ligands by excited states of Ni(II) porphyrins. *Chem. Phys. Lett.* 98:584–589.

Kreszowski, D. H., G. Deinum, and G. T. Babcock. 1994. Picosecond time-resolved resonance Raman scattering from zinc(II)octaethylporphyrin. *J. Am. Chem. Soc.* 116:7463–7464.

Kruglik, S. G., Y. Mizutani, and T. Kitagawa. 1997. Time-resolved resonance Raman study of the primary photoprocesses of nickel(II)octaethylporphyrin in solution. *Chem. Phys. Lett.* 266:283–289.

Lambright, D. G., S. Balasubramanian, and S. G. Boxer. 1991. Protein relaxation dynamics in human myoglobin. *Chem. Phys.* 158:249–260.

Levine, L. M. A., and D. Holten. 1988. Axial-ligand control of the photophysical behavior of ruthenium (II) tetraphenyl- and octaethylporphyrin. Contrasting properties of metalloporphyrin (π, π^*) and (d, π^*) excited states. *J. Phys. Chem.* 92:714–720.

Li, P., J. T. Sage, and P. M. Champion. 1992. Probing picosecond processes with nanosecond laser: electronic and vibrational relaxation dynamics of heme proteins. *J. Chem. Phys.* 97:3214–3227.

Lian, T., B. Locke, Y. Kholodenko, and R. M. Hochstrasser. 1994. Energy-flow from solute to solvent probed by femtosecond IR spectroscopy—malachite green and heme protein solutions. *J. Chem. Phys.* 98: 11648–11656.

Lim, M., T. A. Jackson, and P. A. Anfinrud. 1996. Femtosecond near-IR absorbance study of photoexcited myoglobin: the dynamics of electronic and thermal relaxation. *J. Phys. Chem.* 100:12043–12051.

Lingle, R., Jr., X. Xu, H. Zhu, S. C. Yu, and J. B. Hopkins. 1991. Picosecond Raman-study of energy-flow in a photoexcited heme protein. *J. Phys. Chem.* 95:9320–9331.

Loppnow, G. R., D. Melamed, A. R. Leheny, A. D. Hamilton, and T. G. Spiro. 1993. Excited-state photophysics of donor-appended cobalt(II) porphyrins from picosecond transient absorption spectroscopy. *J. Phys. Chem.* 97:8969–8975.

Martin, J. L., A. Migus, C. Poyart, Y. Lecarpentier, R. Astier, and A. Antonetti. 1983a. Femtosecond photolysis of CO-ligated protoheme and hemoproteins—appearance of deoxy species with a 350-fsec time constant. *Proc. Natl. Acad. Sci. U.S.A.* 80:173–177.

Martin, J. L., A. Migus, C. Poyart, Y. Lecarpentier, R. Astier, and A. Antonetti. 1983b. Spectral evidence for subpicosecond iron displacement after ligand detachment from hemoproteins by femtosecond light-pulses. *EMBO J.* 2:1815–1819.

Mills, F. C., G. K. Ackers, H. T. Gaud, and S. J. Gill. 1979. Thermodynamics studies on ligand binding and subunit association of human hemoglobins. *J. Biol. Chem.* 254:2875–2880.

Mizutani, Y., and T. Kitagawa. 1997. Direct observation of cooling of heme upon photodissociation of carbonmonoxy myoglobin. *Science.* 278:443–446.

Myers, A. B., and R. A. Mathies. 1987. *In* Biological Applications of Raman Spectroscopy. Wiley and Sons, New York.1–58.

Nagai, K., and T. Kitagawa. 1980. Differences in Fe(II)-Ne(His-F8) stretching frequencies between deoxyhemoglobins in the alternative quaternary structures. *Proc. Natl. Acad. Sci. U.S.A.* 77:2033–2037.

Naganuma, K., K. Mogi, and H. Yamada. 1989. General method for ultrashort light-pulse chirp measurement. *IEEE J. Quant. Elec.* 25: 1225–1233.

Nishizawa, E., H. Hashimoto, and Y. Koyama. 1989. Raman spectra of chlorophyll a in the T_1 state. *Chem. Phys. Lett.* 164:155–160.

Perutz, M. F. 1979. Regulation of oxygen affinity of hemoglobin: influence of structure of the globin on the heme iron. *Ann. Rev. Biochem.* 48: 327–386.

Petrich, J. W., J. C. Lambry, S. Balasubramanian, D. G. Lambright, S. G. Boxer, and J. L. Martin. 1994. Ultrafast measurements of geminate recombination of NO with site-specific mutants of human myoglobin. *J. Mol. Biol.* 238:437–444.

Petrich, J. W., J.-L. Martin, D. Houde, C. Poyart, and A. Orszag. 1987. Time-resolved Raman spectroscopy with subpicosecond resolution: vibrational cooling and delocalization of strain energy in photodissociated (carbonmonoxy)hemoglobin. *Biochemistry.* 26:7914–7923.

Petrich, J. W., C. Poyart, and J. L. Martin. 1988. Photophysics and reactivity of heme proteins: a femtosecond absorption study of hemoglobin, myoglobin, and protoheme. *Biochemistry.* 27:4049–4060.

Rodriguez, J., and D. Holten. 1989. Ultrafast vibrational dynamics of a photoexcited metalloporphyrin. *J. Chem. Phys.* 91:3525–3531.

Rodriguez, J., L. McDowell, and D. Holten. 1988. Elucidation of the role of metal-to-ring charge-transfer excited states in the deactivation of photoexcited ruthenium porphyin carbonyl complexes. *Chem. Phys. Lett.* 147:235–240.

Schlichting, I., J. Berendzen, G. N. Phillips, Jr., and R. M. Sweet. 1994. Crystal structure of an intermediate of CO binding to myoglobin. *Nature.* 371:808–812.

Schneebeck, M. C., L. E. Vigil, and M. R. Ondrias. 1993. Mode-selective energy localization during photoexcitation of deoxy hemoglobin and heme model complexes. *Chem. Phys. Lett.* 215:251–256.

Sension, R. J., S. T. Repinec, A. Z. Szarka, and R. M. Hochstrasser. 1993. Femtosecond laser studies of the *cis*-stilbene photoisomerization reactions. *J. Chem. Phys.* 98:6291–6315.

Shreve, A. P., and R. A. Mathies. 1995. Thermal effects in resonance Raman scattering—analysis of the Raman intensities of rhodopsin and the time-resolved Raman scattering of bacteriorhodopsin. *J. Phys. Chem.* 99:7285–7299.

Sorai, M., and S. Seki. 1974. Phonon coupled cooperative low-spin $^1A_1$–high-spin $^5T_2$ transition in $[Fe(phen)_2(NCS)_2]$ and $[Fe(phen)_2(NCSe)_2]$ crystals. *J. Chem. Phys. Solids.* 35:555–570.

Srajer, V., and P. M. Champion. 1991. Investigations of optical line shapes and kinetic hole burning in myoglobin. *Biochemistry.* 30:7390–7402.

Srajer, V., T. Y. Teng, T. Ursby, C. Pradervand, Z. Ren, S. Adachi, W. Schildkamp, D. Bourgeois, M. Wulff, and K. Moffat. 1996. Photolysis of the carbon monoxide complex of myoglobin: nanosecond time resolved crystallography. *Science.* 274:1726–1729.

Stavrov, S. S. 1993. The effect of iron displacement out of the porphyrin plane on the resonance Raman spectra of heme proteins and iron porphyrins. *Biophys. J.* 65:1942–1950.

Tait, C. D., D. Holten, and M. Gouterman. 1984. Picosecond photolysis of axial ligands on cobalt(II) and cobalt(III) porphyrins. *J. Am. Chem. Soc.* 108:6731–6738.

Teng, T.-Y., V. Srajer, and K. Moffat. 1994. Photolysis-induced structural changes in single crystals of carbonmonoxy myoglobin at 40 K. *Nature Struct. Biol.* 1:701–705.

Tsubaki, M., R. B. Srivastava, and N.-T. Yu. 1982. Resonance Raman investigation of carbon monoxide bonding in (carbonmonoxy)hemoglobin and -myoglobin: detection of the Fe-CO stretching and Fe-C-O bending vibrations and influence of the quaternary structure change. *Biochemistry.* 21:1132–1140.

Vitols, S. E., R. Kumble, M. E. Blackwood, Jr., J. S. Roman, and T. G. Spiro. 1995. Charge transfer switching in photoexcited Ru(II) porphyrins: a time-resolved resonance Raman and spectroelectrochemical study. *J. Phys. Chem.* submitted

Vogler, A., and H. Kunkely. 1976. Photochemistry of biologically important transition metal complexes. II Carbonylpiperidinetetraphenylporphine complexes of iron(II) and ruthenium(II). *Ber. Bunsenges. Phys. Chem.* 80:425.

Walda, K. N., X. Y. Liu, V. S. Sharma, and D. Magde. 1994. Geminate recombination of diatomic ligands CO, O_2, and NO with myoglobin. *Biochemistry.* 33:2198–2209.

Waleh, A., and G. H. Loew. 1982. Quantum mechanical studies of the photodissociation of carbonylheme complexes. *J. Am. Chem. Soc.* 104: 2346–2351.

Wells, A. V., T. J. Sage, D. Morikis, P. M. Champion, M. L. Chiu, and S. G. Sligar. 1991. The iron-histidine mode of myoglobin revisited: resonance Raman studies of isotopically labeled *Escherichia coli* expressed myoglobin. *J. Am. Chem. Soc.* 113:9655–9660.

Yamaguchi, S., and H. Hamaguchi. 1995. Convenient method of measuring the chirp structure femtosecond white-light continuum pulses. *Appl. Spec.* 49:1513–1515.

Zerner, M., M. Gouterman, and H. Kobayashi. 1966. Porphyrins VIII. Extended Huckel calculations on iron complexes. *Theor. Chim. Acta.* 6:383–400.

Zhu, L. Y., G. Zhong, M. Unno, S. G. Sligar, and P. M. Champion. 1996. Femtosecond coherence spectroscopy of heme proteins. *Biospectroscopy.* 2:301–309.